Terahertz quantum cascade lasers with double-resonant-phonon depopulation

Benjamin S. Williams, Sushil Kumar, Qi Qin, et al.

View Online   Export Citation

ARTICLES YOU MAY BE INTERESTED IN

Terahertz quantum cascade lasers with double-resonant-phonon depopulation

Benjamin S. Williams,[a] Sushil Kumar, Qi Qin, and Qing Hu
Research Laboratory of Electronics, Department of Electrical Engineering and Computer Science, Massachusetts Institute of Technology, Cambridge, Massachusetts 02139

John L. Reno
Sandia National Laboratories, Department 1123, MS 0601, Albuquerque, New Mexico 87185-0601

We present two different terahertz quantum cascade laser (QCL) designs based on GaAs/Al$_{0.3}$Ga$_{0.7}$As heterostructures that feature a depopulation mechanism of two longitudinal-optical phonon scattering events. This scheme is intended to improve high temperature operation by reducing thermal backfilling of the lower radiative state. The better of these two devices displays a threshold current density of 170 A/cm^2 at 5 K and lases up to 138 K in pulsed mode and 105 K in continuous-wave mode. However, contrary to expectation, we observed no improvement in temperature performance compared to single-resonant-phonon designs, which suggests that the thermal backfilling is not yet a limiting factor for high temperature terahertz QCL operation. © *2006 American Institute of Physics.* [DOI: 10.1063/1.2216112]

Terahertz quantum cascade lasers (QCLs) have recently become available as continuous-wave (cw) sources of coherent radiation that presently cover the frequency range of 1.9–5.0 THz ($\lambda \sim 60$–161 μm).[1,2] The best temperature performance for terahertz QCLs has been demonstrated using metal-metal waveguides with the resonant-phonon depopulation scheme,[3] which has allowed operation up to 164 K in pulsed mode and 117 K in cw mode.[4] In this respect terahertz QCLs suffer by comparison with their elder cousins in the mid-infrared (with frequencies above the reststrahlen band), for which robust room-temperature cw operation has been demonstrated at wavelengths from 4 to 9 μm.[5,6] It was recognized early in the development of QCLs that thermal backfilling of the lower radiative state by carriers from the heavily populated injector states could effectively lengthen the lower state lifetime τ_l and degrade population inversion; the injector regions were therefore typically designed with large energy separations ($\Delta \geq 100$ meV) between the lower lasing level and the ground state.[7] More recently, mid-IR quantum cascade active regions with doubly resonant longitudinal-optical (LO) phonon depopulation schemes have been used to demonstrate room-temperature cw operation.[5,6,8] In this letter, we present results from two QCLs designed for terahertz frequency operation that incorporate double-resonant-phonon depopulation.

Considering a simple two-level model for intersubband lasers, the gain can be described by the expression $g \propto f_{ul} \tau_u (1 - \tau_l / \tau_{ul})$, where f_{ul} is the transition oscillator strength, τ_{ul} is the scattering time from the upper to lower state, and τ_u and τ_l are the overall lifetimes of the subbands. In addition to thermal backfilling mentioned above, which increases τ_l, the other principal temperature degradation mechanism is the onset of thermally activated LO-phonon scattering, as electrons acquire sufficient in-plane energy to emit a LO phonon and relax to the lower subband. This causes the upper state lifetime to decrease as $\tau_{ul} \propto \exp[(\hbar\omega - E_{LO})/k_B T_e]$, where $\hbar\omega$ is the terahertz photon energy and

E_{LO} is the LO-phonon energy (36 meV in GaAs). This is a fundamental feature of terahertz QCLs, where $\hbar\omega < E_{LO}$. Both mechanisms sensitively depend on the electron gas temperature T_e, which numerical simulations as well as measurements suggest to be 50–100 K higher than the lattice temperature during device operation.[9,10] In a typical terahertz resonant-phonon structure, the injector states are separated from the lower radiative state by approximately $\Delta \approx E_{LO}$ in order to facilitate fast resonant LO-phonon scattering,[11] as well as to serve as the activation energy barrier against the thermal backfilling process. Therefore, by following the example set by the mid-IR QCLs, one might expect that incorporating a double-phonon depopulation scheme would improve high temperature performance by increasing Δ compared to T_e and by preventing the excitation of carriers from the injector states by reabsorption of nonequilibrium LO phonons (hot-phonon effect).[12]

The conduction band and energy level schematics for both two-phonon designs are shown in Fig. 1. The conduction band diagram, energy levels, and wave functions were calculated using a one-dimensional Schrödinger solver, where band nonparabolicity was accounted for using an energy dependent effective mass model.[13] Both devices were grown by molecular beam epitaxy with GaAs/Al$_{0.3}$Ga$_{0.7}$As quantum wells. In both devices, the radiative transition takes place between the upper and lower levels labeled u and l. For device A (labeled FTP104, wafer EA1126), the LO-phonon depopulation scattering events take place in two separate wide wells, which are connected by a four-state miniband with a bandwidth of approximately 14 meV. The thicknesses of the barriers in this miniband were chosen in an attempt to provide fast transport between the wide wells, but thick enough to suppress parasitic coupling between the upper radiative state and any excited states close in energy. In terms of energy level design and applied field ($\sim$10 kV/cm at design bias), device A is very similar to a standard resonant-phonon structure,[4] except with three extra wells added per module to allow a second phonon depopulation event. Device B (FTP185C, wafer EA1267), on the other hand, is designed to operate at a higher field ($\sim$17 kV/cm) and with

---
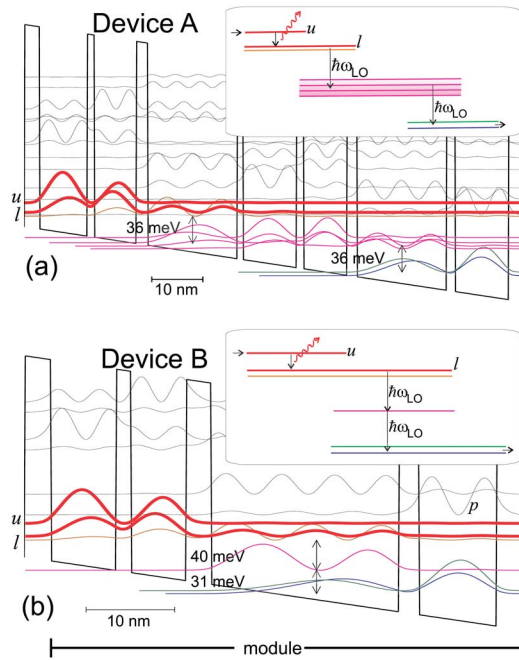[a]Electronic mail: bwilliam@mit.edu

FIG. 1. (Color online) Calculated conduction band diagrams and level schematics for devices A and B. For device A, the layer thicknesses in Å are 31/93/14/82/23/175/11/105/14/85/20/175/17/105, with the underlined layer doped at $n=2.8\times10^{16}$ cm^{-3}. For device B, the thicknesses are 31/73/17/62/28/212/23/88, with the underlined layer doped at $n=1.4\times10^{16}$ cm^{-3}.

FIG. 3. (Color online) Optical power vs current characteristics for device B measuring 40 μm $\times$ 1.23 mm. Measurements were taken with 200 ns pulses repeated at 10 kHz (upper panel) and in cw mode (lower panel). The upper inset displays typical cw spectra, and the lower inset contains *V-I* and *dV/dI-I* characteristics at 7, 74, and 102 K.

a single wide well so that both LO-phonon relaxation events take place within a single quantum well. In theory, this should allow a more efficient depopulation, as the resonant tunneling through the miniband in device A may slow the relaxation process. Because of the intrinsic energy level spacings in a single quantum well, the subband separations in the wide quantum well are not exactly equal, but their sum is close to $2E_{LO}$. The calculated lower state lifetimes due to LO-phonon scattering are $\tau_l=0.5$ ps for device A and $\tau_l=0.35$ ps for device B.

Device A was grown with 104 repeated modules and device B with 185 modules to form active regions approximately 10 μm thick. Both devices were grown with cap lay-ers and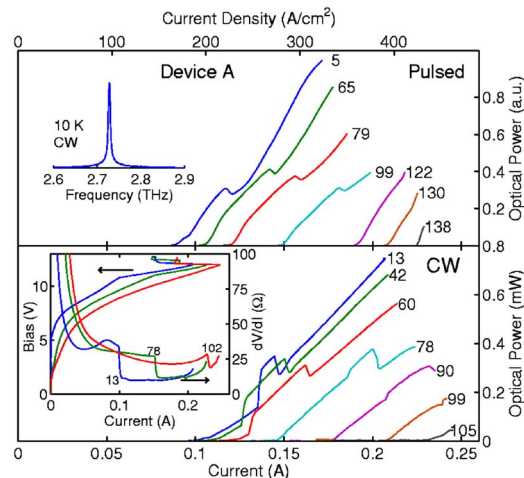 etch stop layers described in Ref. 4 and were fabricated into metal-metal waveguides using copper-to-copper thermocompression wafer bonding.[4] Laser ridges were cleaved and mounted using indium solder on copper heat sinks on a cold plate in a vacuum cryostat. No facet coatings were used, and power was collected by placing the small aperture of a Winston cone close to one facet and measured by a thermopile detector (Scientech AC2500H).

The light versus current (*L-I*) characteristics were collected in both pulsed and cw modes from device A and are plotted in Fig. 2. In pulsed mode, the threshold current was $J_{th}=170$ A/cm^2 at 10 K, and lasing continued up to a maximum temperature of $T_{max}=138$ K. Lasing ceases at the maximum current J_{max} when the injection subbands become misaligned, and the device enters into a negative differential resistance (NDR) region. In cw mode, lasing took place at 2.73 THz with $J_{th}=185$ A/cm^2 at 10 K and a maximum power of 0.75 mW. Two notable features can be seen in the cw voltage versus current (*V-I*) and differential resistance versus current (*dV/dI-I*) characteristics plotted in the inset of Fig. 2. First, at 13 K a dip in the differential resistance at 0.05 A reveals the presence of a subthreshold parasitic leakage channel; lasing does not occur until the device is biased beyond this point. Second, at the onset of lasing the clamping of the population inversion is reflected by a sharp kink in the *V-I* curve and a large discontinuity (72% at 13 K) in the

FIG. 2. (Color online) Optical power vs current characteristics for device A with a width of 50 μm and length of 1.06 mm. Measurements were taken at different heat-sink temperatures with 200 ns pulses repeated at 10 kHz (upper panel) and in cw mode (lower panel). The upper inset displays a typical cw emission spectrum, and the lower inset displays cw *V-I* and *dV/dI-I* characteristics at 13, 78, and 102 K.
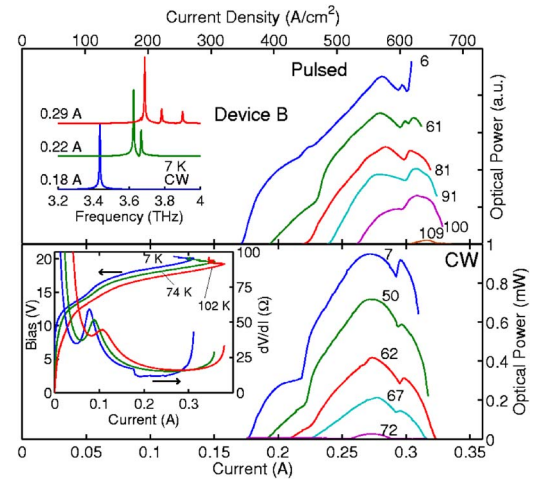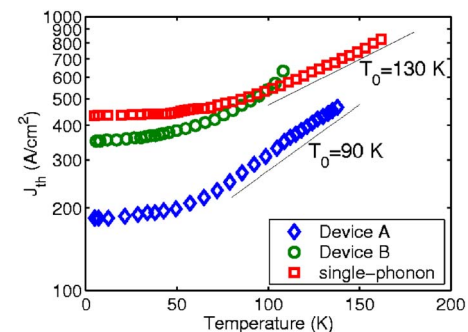

FIG. 4. (Color online) Pulsed threshold current densities vs temperature for device A and B as well as for a 2.9 THz single-resonant-phonon device described in Ref. 4. Fits to the expression $J_{th} \propto \exp(T/T_0)$ are given as guides for the eye.

differential resistance. This reflects a large ratio between the upper and lower state lifetimes and indicates highly selective injection and depopulation processes.[14]

Measured *L-I* characteristics and spectra from device B are presented in Fig. 3. $J_{th}=350$ A/cm^2 in pulsed mode and lasing continued up to $T_{max}=109$ K. At 7 K in cw mode, $J_{th}=360$ A/cm^2 with a peak power of 0.95 mW, and the device lased at various modes from 3.4 to 3.7 THz. Examination of the *V-I* curve (Fig. 3, inset) reveals that the NDR occurs at a relatively high voltage ($\sim$20 V) because of the larger designed field for this structure.

Despite our expectations, these two devices show no particular temperature improvement compared to the best performance from single-resonant-phonon designs, which typically lase up to 130–170 K in pulsed mode.[3,4] In fact, device B exhibits particularly poor temperature performance ($T_{max}=109$ K) compared to the expectation that a vertical intrawell two-phonon transition would provide a more efficient electron relaxation than device A. The values of J_{th} measured in pulsed mode are plotted versus temperature for both devices in Fig. 4 as well as for the single-resonant-phonon device described in Ref. 4. While all of these lasers have similar dynamic range for lasing current ($J_{max}/J_{th}\sim2$), the two-phonon devices degrade more quickly with temperature, i.e., they have smaller characteristic temperatures T_0, where $J_{th}\propto\exp(T/T_0)$ at high temperatures.

For device A, we believe that the faster than typical increase of J_{th} with temperature is due to the strong temperature dependence of the subthreshold parasitic channel. In effect, the low threshold of $J_{th}=170$ A/cm^2 (compared to $J_{th}=300–500$ A/cm^2 for previous single-resonant-phonon lasers) may not necessarily be due to intrinsically better depopulation or more gain, but rather a better suppression of parasitic leakage current at low temperatures. This is consistent with the well documented reduction of J_{th} that has accompanied our previous attempts to suppress this parasitic channel.[3,4,11] If we accept the proposition that J_{th} is limited by this subthreshold leakage current, then the fast increase in the parasitic channel current with temperature (see the *V-I* curve in Fig. 2) would cause a corresponding fast increase in J_{th}. The reason for this dependence likely has to do with the nature of the four-state miniband that couples the two-phonon scattering events. At low biases the miniband is not completely aligned, its states are more localized in their respective wells, and transport will be inhibited. At higher temperatures the Fermi distribution of electrons becomes broader and transport through the miniband becomes more efficient, which pushes up the parasitic channel and thus also J_{th}. This mechanism is also likely the cause of the strong increase in J_{max} with temperature (see Fig. 2, upper panel), which is somewhat unusual for a resonant-phonon laser.

While device B also suffers from a low T_0 value, this cannot be blamed on a subthreshold leakage channel. Examination of the transport characteristics reveals that the parasitic channel indicated by the minimum in the *dV/dI-I* at $I\sim0.05$ A barely increases in current between 7 and 74 K, by which point lasing has already ceased. This is because the intrawell two-phonon design has no miniband structure in the middle of the module to selectively impede current flow. However, there is likely a problem with a different type of parasitic coupling—coupling of the upper radiative state with a higher energy state [labeled "p" in Fig. 1(b)]. Because of the high field applied to this structure, this state is only

12 meV above the upper radiative state, which is much closer than in a single-phonon structure where this gap is typically 20–30 meV. Thermal excitation of carriers to p creates a parasitic current channel and would reduce the upper state lifetime. This is consistent with the roll-off of the *L-I* curve before the NDR, and with the small discontinuity in the *dV/dI-I* characteristic (32% at 7 K) which indicates a smaller lifetime ratio τ_u/τ_l, and is contrary to expectations for this intrawell two-phonon design.

These results suggest that for the current generation of resonant-phonon devices, depopulation of the lower state is not yet the limiting factor for performance—at least for the temperatures reached thus far ($\sim$170 K). Improvements in depopulation efficiency in the two devices reported here appear to have been offset by either a strongly temperature dependent subthreshold leakage channel (device A) or a reduced upper state lifetime τ_u due to parasitic coupling with a low-lying excited state (device B). This suggests that on the immediate path to higher temperature operation it is more important to focus on preserving a long upper state lifetime. This is not entirely unexpected, since while τ_u is degraded by thermally activated LO-phonon scattering and τ_l is degraded by thermal backfilling, the activation energy of the former process ($E_{LO}-\hbar\omega$) is smaller than that for the latter ($\Delta\sim E_{LO}$), and so an earlier onset would be expected for the former. This conclusion is further supported by the recent room-temperature operation of a mid-infrared "injectorless" QCL with a small barrier of only $\Delta\sim36$ meV even though its dissipation power density is $\sim$100 times larger than our own terahertz QCLs—which demonstrates that a large energy barrier to thermal backfilling is not strictly necessary for high temperature operation.[15]

[1] R. Köhler, A. Tredicucci, F. Beltram, H. E. Beere, E. H. Linfield, A. G. Davies, D. A. Ritchie, R. C. Iotti, and F. Rossi, Nature (London) **417**, 156 (2002).
[2] S. Kumar, B. S. Williams, Q. Hu, and J. L. Reno, Appl. Phys. Lett. **88**, 121123 (2006).
[3] Q. Hu, B. S. Williams, S. Kumar, H. Callebaut, S. Kohen, and J. L. Reno, Semicond. Sci. Technol. **20**, S228 (2005).
[4] B. S. Williams, S. Kumar, Q. Hu, and J. L. Reno, Opt. Express **13**, 3331 (2005).
[5] M. Beck, D. Hofstetter, T. Aellen, J. Faist, U. Oesterle, M. Ilegems, E. Gini, and H. Melchior, Science **295**, 301 (2002).
[6] J. S. Yu, S. R. Darvish, A. Evans, J. Nguyen, S. Slivken, and M. Razeghi, Appl. Phys. Lett. **88**, 041111 (2006).
[7] C. Sirtori, J. Faist, F. Capasso, D. L. Sivco, A. L. Hutchinson, S. N. G. Chu, and A. Y. Cho, Appl. Phys. Lett. **68**, 1745 (1995).
[8] J. Faist, D. Hofstetter, M. Beck, T. Aellen, M. Rochat, and S. Blaser, IEEE J. Quantum Electron. **38**, 533 (2002).
[9] H. Callebaut, S. Kumar, B. S. Williams, Q. Hu, and J. L. Reno, Appl. Phys. Lett. **84**, 645 (2004).
[10] M. S. Vitiello, G. Scamarcio, V. Spagnolo, B. S. Williams, S. Kumar, Q. Hu, and J. L. Reno, Appl. Phys. Lett. **86**, 111115 (2005).
[11] B. S. Williams, H. Callebaut, S. Kumar, Q. Hu, and J. L. Reno, Appl. Phys. Lett. **82**, 1015 (2003).
[12] J. T. Lü and J. C. Cao, Appl. Phys. Lett. **88**, 061119 (2006).
[13] R. P. Leavitt, Phys. Rev. B **44**, 11270 (1991).
[14] C. Sirtori, F. Capasso, J. Faist, A. L. Hutchinson, D. L. Sivco, and A. Y. Cho, IEEE J. Quantum Electron. **34**, 1722 (1998).
[15] A. Friedrich, G. Boehm, M. C. Amann, and G. Scarpa, Appl. Phys. Lett. **86**, 161114 (2005).